Macromolecular assembly and membrane activity of antimicrobial *D,L*-α-Cyclic peptides

Bárbara Claro[1], Antonio Peón[1], Eva González-Freire[2], Erik Goormaghtigh[3], Manuel Amorín[2], Juan R. Granja[2], Rebeca Garcia-Fandiño*[1,2], Margarida Bastos*[1]

[1]CIQUP, Centro de Investigação em Química, Departamento de Química e Bioquímica, Faculdade de Ciências, Universidade do Porto, Porto, Portugal;

[2]Centro Singular de Investigación en Química Biolóxica e Materiais Moleculares (CiQUS), Departamento de Química Orgánica, Universidade de Santiago de Compostela, 15782 Santiago de Compostela, Spain

[3]Structure and Function of Biological Membranes, Center for Structural Biology and Bioinformatics, ULB, Brussels, Belgium

KEYWORDS. Antimicrobial Peptides, *D,L*-α-cyclic peptides, Self-Assembled Cyclic Peptide Nanotubes, Differential Scanning Calorimetry, polarized ATR-FTIR, Coarse-Grained Molecular Dynamics Simulations.

Statistical summary of the article:

Total number of words in main text – 6336

Figures - 8

Abstract

Antimicrobial peptides are viewed as a promising alternative to conventional antibiotics, as their activity through membrane targeting makes them less prone to resistance development. Among them, antimicrobial *D,L*-α-cyclic peptides (CPs) have been proposed as an alternative, specially due to their cyclic nature and to the presence of *D*-amino acids that increases their resistance to proteases. In present work, second generation *D,L*-α-cyclic peptides with proven antimicrobial activity are shown to form complex macromolecular assemblies in the presence of membranes. We addressed the CPs:membrane interactions through a combination of experimental techniques (DSC and

ATR-FTIR) with Coarse grained molecular dynamics (CG-MD) simulations, aiming at understanding their interactions, macromolecular assemblies and eventually unveil their mechanism of action. DSC shows that the interaction depends heavily on the negatively charge content of the membrane and on lipid/peptide ratio, suggesting different mechanisms for the different peptides and lipid systems. CG-MD proved that CPs can self-assemble at the lipid surface as nanotubes or micellar aggregates, depending on the peptide, in agreement with ATR-FTIR results. Finally, our results shed light into possible mechanisms of action of the peptides with pending hydrocarbon tail, namely membrane extensive segregation and/or membrane disintegration through the formation of disk-like lipid/peptide aggregates.

1. Introduction

The development of new, intelligent nanomaterials, capable of self-organization replying to external stimuli, has been studied in the recent years, and a number of different applications can be found in the literature [1-6]. Although a variety of different materials have been studied, the structural similarity with natural peptides and proteins that are the main molecular building blocks in nature makes the use of peptide-derived materials the most common approach towards biocompatibility [7-9]. Some of these peptide-derived new molecules were shown to self-assemble into structures such as nanotubes, due their broad conformational, chemical and functional features [10-12]. One such group of compounds are supramolecular structures called self-assembling cyclic peptide nanotubes (SCPNs), build from cyclic peptides (CPs) with an even number of alternating *D*- and -*L*-α-amino acids, as illustrated by Ghadiri and co-workers [3]. These new materials have been shown to be able to form artificial transmembrane channels for ions, or to act as good alternative to antimicrobial candidates, depending on peptide side chains composition and hydrophobicity [3, 13-15]. These *D*,*L*-α-cyclic peptides (*D*,*L*-α-CPs) can adopt a planar ring structure with side chains pointing outwards of the nanotube. Within the appropriate environment, individual CPs can stack in a *β*-sheet structure, creating intermolecular hydrogen bond networks along the growing axis, forming the SCPNs [11, 16].

Antimicrobial resistance is considered as one of the major global health issues of the 21st century [17], as the current therapeutic strategies are no longer appropriate to fight infection and drug-resistant pathogens. In this combat, antimicrobial peptides (AMPs),

also known as host defense peptides [18], are currently in the spotlight as a good alternative to the conventional therapeutics to overcome bacterial resistance, as their main target is the bacterial membrane and they induce significantly lower resistance [19]. AMPs are produced by a variety of organisms and present a diversity of functional and structural properties [20, 21], but exhibit common basic features - they are usually cationic, with amphipathic structure, they have a small number of amino acids and they are active against Gram-positive and Gram-negative bacteria, fungi and viruses [20, 21]. Different mechanisms of action have been proposed for AMPs [22-24], all causing membrane perturbation and/or destruction. Their action is triggered by electrostatic interactions, the first driving force for interaction with the membranes, as the cationic AMPs interact with the anionic membrane surface (negative headgroups) of pathogens. Thereafter there is usually accumulation and rearrangement at the membrane, leading to membrane micellization, segregation/permeabilization, pore formation or aggregation [25-27]. Amphipathic cationic *D*,*L*-α-CPs, have been shown to be potent antimicrobials whose mechanism of action is related with the nanotube formation that is facilitated by membrane interaction, being this supramolecular structure the main active form [28]. The robust secondary structure allied with the presence of *D*-amino acid residues reduces the resistance against proteases, making SCPNs promising antimicrobial candidates [13, 14, 16, 29-31]. Therefore, the design of new SCPNs with good antimicrobial activity is a very attractive application of these peptides, for their possible significant contribution to worldwide wealth.

We combined experimental techniques (differential scanning calorimeter (DSC) and attenuated total reflection Fourier transform infrared spectroscopy (ATR-FTIR)) with coarse-grained Molecular Dynamics simulations (CG-MD) to characterize and rationalize the interactions of three second generation CPs of proven antimicrobial activity [32] with lipid model membranes.

The antimicrobial *D*,*L*-α-CPs used in this study are designated as **CPR,** *c*-[RSKSWPgKQ] , **CPRT10,** *c*-[RSKSWX^{C10}KQ] and **CPRT14,** *c*-[RSKSWX^{C14}KQ] (Fig. 1), and were designed as second generation peptides, based on a CP previously reported by our group, there called CP2 [13]. In the amino acid sequence the use of brackets indicates that the peptides have a cyclic structure, the underlined amino acids are *D*-amino acids and X denotes (*S*)-2-amino-3-(1λ^2,2,3-triazol-4-yl) propanoic acid. **CPR**, **CPRT10** and **CPRT14** are soluble in water and they contain one hydrophobic residue

(tryptophan (W)), known to increase membrane anchoring, three charged residues (one arginine (R) and two lysines (K)), and three polar non-charged residues (one glutamine (Q) and two serines (S)). **CPRT10** and **CPRT14** differ from **CPR** as they have a ten (T10) and fourteen (T14) carbons' tails, respectively, linked to the propargylglycine group (Pg) through a copper catalyzed azide–alkyne cycloaddition (CuAAC reaction). All three CPs present good antimicrobial activity, mainly against Gram positive bacteria [32].

DMPE (1,2-dimyristoyl-*sn*-glycero-3-phosphoethanolamine) and DMPG (1,2-dimyristoyl-*sn*-glycero-3-phospho-(1'-rac-glycerol)) are used as simple models for the bacterial membrane, since they are known to have a significant presence in Gram-negative and Gram-positive bacteria cytosolic membrane. Although the lipid composition varies quite significantly among pathogens, typically Gram-negative bacteria have a higher PE content and Gram-positive bacteria a higher PG content [33]. As our peptides showed the highest activity towards Gram-positive bacteria [32], we chose mixture with high PG content, *i.e.*, pure DMPG membranes and mixtures of DMPE:DMPG at different molar ratios (1:1) and (1:9). Further to these, we also used DMPE alone, to assess its role on the interactions of the peptides with the lipid mixtures. Finally eukaryotic membranes were mimicked by using 1,2-dimyristoyl-*sn*-glycero-3-phosphocholine (DMPC), as a control for toxicity, as has been seen in different studies a remarkable correlation between toxicity and DSC AMP:PC profile [26, 34-39].

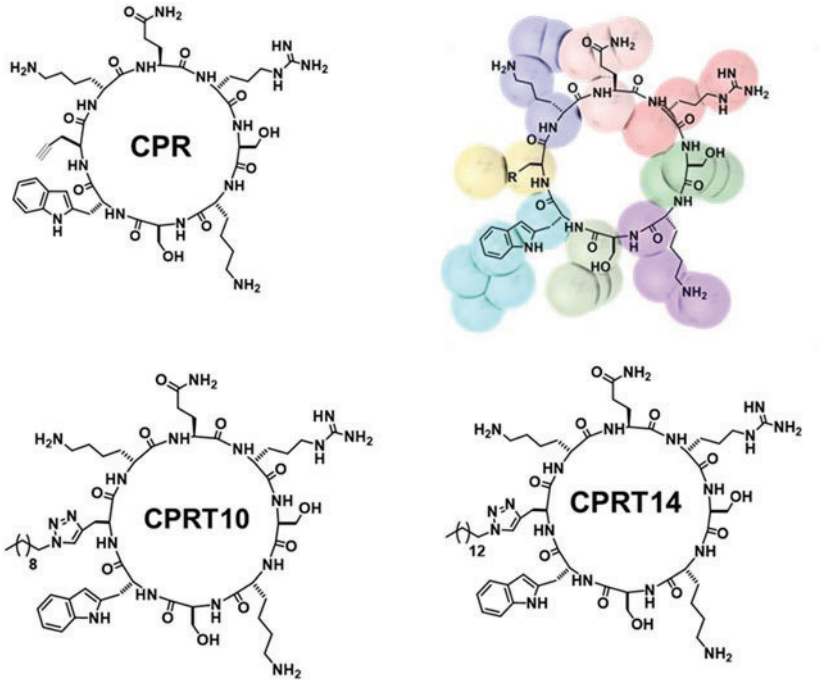

Fig. 1. Structures of the peptides studied here: **CPR,** *c*-[RSKSWPgKQ], **CPRT10,** *c*-[RSKSWX^{C10}KQ] and **CPRT14,** *c*-[RSKSWX^{C14}KQ]. In the amino acid composition here shown the use of brackets indicates that the peptides have a cyclic structure, the underlined amino acids are *D*-amino acids and X denotes (*S*)-2-amino-3-(1λ^2,2,3-triazol-4-yl) propanoic acid. The beads of a Coarse-Grained model for the Molecular Dynamics simulation are represented for **CPR**. Amino acid residues are colored as follow: Gln-1 (rose), Arg-2 (brick-red), Ser-3 (dark green), Lys-4 (violet), Ser-5 (soft green), Trp-6 (cyan), R tail (gold), Lys-8 (dark blue).

2. Experimental

2.1 Materials and Methods

Hexafluorophosphate benzotriazole tetramethyl uronium (N-HBTU), tetrafluoroborate benzotriazole tetramethyl uronium (N-TBTU), and the α-amino acids were purchased from Iris Biotech, Novabiochem, Advanced Chemtech, Aldrich, and/or GL Biochem (Shangai) Ltd. Rink Amide resin was purchased from Novabiochem. Triisopropylsilane (TIS) and diisopropylethylamine (DIEA) were purchased from Sigma-Aldrich, Germany. All solvents were HPLC grade purchased from Aldrich or Fisher Scientific, and they were

used without additional purification, except the dry DCM, which were distilled with CaH_2. Synthesis grade DMF was used to synthesize the peptides on solid phase. 1,2-dimyristoyl-sn-glycero-3-phosphocholine (DMPC), 1,2-dimyristoyl-sn-glycero-3-phosphoethanolamine (DMPE) and 1,2-dimyristoyl-sn-glycero-3-phospho-(1'-rac-glycerol) (DMPG) were from Avanti Polar Lipids, Alabama, USA, and used as received. The water used was in all cases high purity Millipore water. The buffer was prepared with HEPES, NaCl, NaN_3 and EDTA all purchased from Sigma-Aldrich, Germany.

2.1.1. Synthetic procedures

Peptides **CPR**, **CPRT10** and **CPRT14** were synthesized manually by standard Fmoc solid phase peptide synthesis protocols [40-43]. See Supplementary Material for details about synthetic procedure and CPs characterization.

2.1.2. Preparation of Liposomes

Liposomes of DMPE, DMPG and DMPC and their mixtures at different molar ratios were prepared by the lipid film method, as described in detail in Supplementary Material. Large unilamellar vesicles (LUVs) were prepared for all systems except for DMPE, where multilamellar vesicles (MLVs) were used.

2.1.3. Differential Scanning Calorimetry

Differential Scanning Calorimetry measurements were performed in a MicroCal VP-DSC microcalorimeter from Malvern (Worcestershire, UK), by following the same protocol as published by our group before [13, 38]. After the first DSC scan full equilibration was attained, and from the second all scans were identical, as common in similar studies [13, 38, 44]. Therefore, all presented results are for the second scan. The data obtained were treated and integrated after baseline correction, either as one peak or using multi-peak deconvolution. Details on the procedure can be found in Supplementary Material.

2.1.4. Coarse-grained Molecular Dynamics simulations

Coarse-grained molecular dynamics (CG-MD) simulations of **CPR**, **CPRT10** and **CPRT14** interacting with membrane models of DMPE, DMPG and their mixtures were carried out, for at least 2 μs in each case. The CG parameters used for CPs were those corresponding to the polarizable MARTINI force field (Martini v2.2 polar amino acids

and polarizable water) [45, 46], together with the use of distance restraints between all the backbone particles to maintain the cyclic conformation (Fig. 1). The CG topologies for the CPs were built using the martinize.py tool [47] and subsequently modified using local code. Computational details can be found in Supplementary Material.

2.1.5. Attenuated Total Reflection Fourier Transform Infrared Spectroscopy

ATR-FTIR measurements followed the same protocol as published before [13, 48]. The measurements were carried in a Spectrum Two FTIR Spectrometer (PerkinElmer, EUA) equipped with diamond internal reflection element from GladiATR Accessory S2PE (PIKE Technologies Inc, EUA). The details of the procedure can be found in Supplementary Material.

3.1. Results

The DSC thermograms for each model membrane system, as well as for their mixtures with **CPR**, **CPRT10** and **CPRT14** at different L:P ratios can be found in Fig. 2. As expected, the peaks for the pure lipids (DMPG and DMPE) are thinner than the ones observed for their mixtures. The thermodynamic parameters retrieved after baseline correction and integration (T_m and $\Delta_{trans}H$) are presented in Table S1. The values obtained for the pure lipids (DMPE, DMPG and DMPC (Fig. S1, Table S2)) as well as their mixtures agree with the literature [26, 34, 35, 37, 49, 50].

.

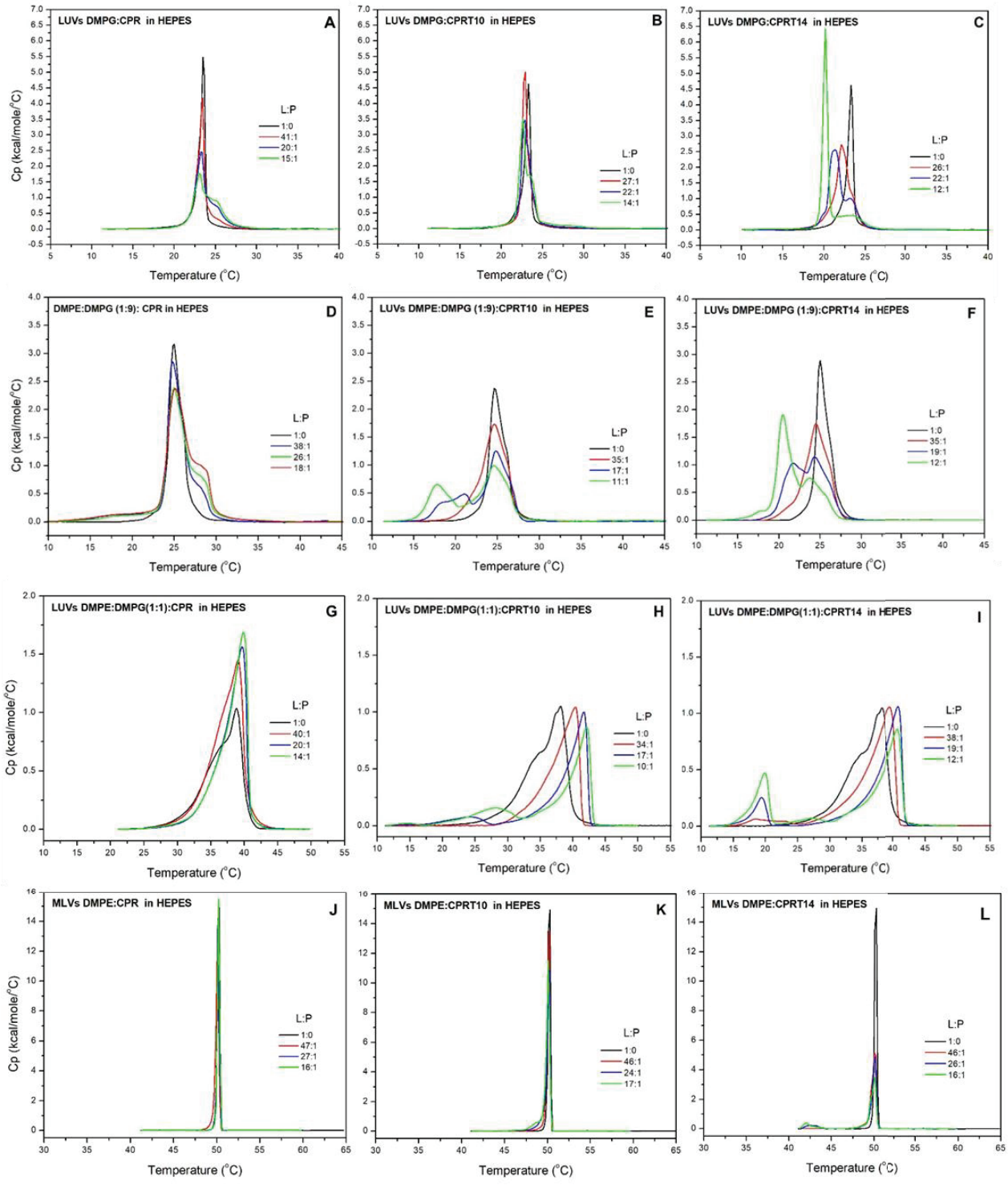
LUVs DMPG:CPR in HEPES
A
L:P
1:0
41:1
20:1
15:1
LUVs DMPG:CPRT10 in HEPES
B
L:P
1:0
27:1
22:1
14:1
LUVs DMPG:CPRT14 in HEPES
C
L:P
1:0
26:1
22:1
12:1
DMPE:DMPG (1:9): CPR in HEPES
D
L:P
1:0
38:1
26:1
18:1
LUVs DMPE:DMPG (1:9):CPRT10 in HEPES
E
L:P
1:0
35:1
17:1
11:1
LUVs DMPE:DMPG (1:9):CPRT14 in HEPES
F
L:P
1:0
35:1
19:1
12:1
LUVs DMPE:DMPG(1:1):CPR in HEPES
G
L:P
1:0
40:1
20:1
14:1
LUVs DMPE:DMPG(1:1):CPRT10 in HEPES
H
L:P
1:0
34:1
17:1
10:1
LUVs DMPE:DMPG(1:1):CPRT14 in HEPES
I
L:P
1:0
38:1
19:1
12:1
MLVs DMPE:CPR in HEPES
J
L:P
1:0
47:1
27:1
16:1
MLVs DMPE:CPRT10 in HEPES
K
L:P
1:0
46:1
24:1
17:1
MLVs DMPE:CPRT14 in HEPES
L
L:P
1:0
46:1
26:1
16:1
Cp (kcal/mole/°C)
Temperature (°C)

Fig. 2. DSC curves for mixtures of the three cyclic peptides **CPR** (left panel), **CPRT10** (middle panel) and **CPRT14** (right panel) with model membranes of DMPG, DMPE and their mixtures. A,B,C: LUVs of DMPG; D,E,F: LUVs of DMPE:DMPG (1:9); G,H,I: LUVs of DMPE:DMPG (1:1); J,K,L: MLVs of DMPE. The molar ratios of lipid to peptide (L:P) for each curve are shown in each plot. The DSC profiles shown are all for the second scan. Note that the y scales for the different lipid systems are different.

In order to try to further decipher the mechanism of action of **CPR**, **CPRT10** and **CPRT14**, CG-MD simulations of 160 CP units placed randomly (representing a molar ratio of lipid to peptide 3:1), were carried out in the presence of the same membrane compositions that were studied experimentally: DMPG, DMPE:DMPG (1:9), DMPE:DMPG (1:1) and DMPE.

The CG-MD simulations show a significant difference in the behavior of the peptide **CPR** when compared to those bearing a hydrophobic tail, **CPRT10** and **CPRT14**, in agreement with the DSC results. The most remarkable contrast is that whereas **CPR** units self-assemble into small or medium-size nanotubes (up to 5 CP units), the presence of T10 and T14 tails induce the formation of mostly micellar aggregates in **CPRT10** and **CPRT14**. In these micellar assemblies, the CPs are acting as the hydrophilic "head" regions in contact with surrounding solvent, sequestering the hydrophobic tail regions in the micelle center (Fig. 3 and Fig. S3-S6).

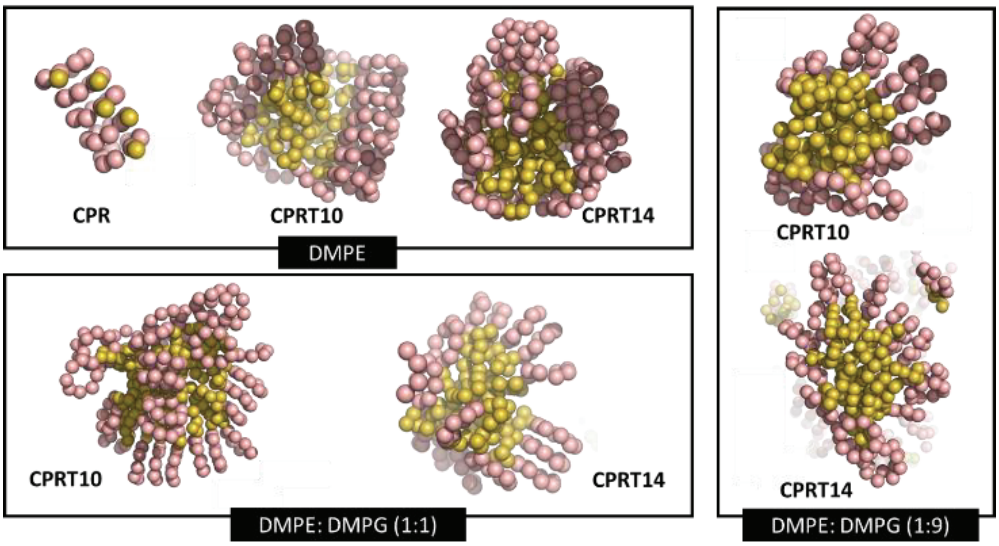

Fig. 3. Detail of some structures found in the last snapshot (t=2 μs) of the CG-MD simulations of **CPR**, **CPRT10** and **CPRT14** in presence of different membrane compositions.

With ATR-FTIR we could characterize experimentally the CPs self-assembly when interacting with the model membranes of DMPG, DMPE:DMPG (1:9) and DMPE:DMPG (1:1). The use of polarized ATR-FTIR allowed us to assess their orientation relative to the membrane plane. The amide I band peaks support the presence of β-sheet/aggregated structures whereas the amide II peak indicates intermolecularly interactions. The results obtained can be found in Fig. 6,7 and 8 and in Fig. S9 and S10.

3.2. Discussion

DMPG and DMPE:DMPG (1:9) model membranes

As stated above, the behavior of **CPR** is different from the obtained for the other two peptides with tail, **CPRT10** and **CPRT14**. When **CPR** is mixed with lipid systems with high PG content, the DSC results (Fig. 2A for pure DMPG and 2D for DMPE:DMPG (1:9)) reveals a small shoulder above the T_m (25ºC), but the temperature for the main transition is maintained (Table S1). The relative importance of the shoulder increases, representing almost half of the total enthalpy change for the largest peptide content. This suggests a phase separation into peptide-poor and peptide-rich domains in the membrane, as also found previously by Sevcsik *et al* [51]. These authors confirmed by X-ray that the shoulder reflects the presence of a quasi-interdigitated phase, which creates a void in the membrane that is compensated by moving the inner lipid layer towards the hydrophobic part of the peptide nanotube. Altogether, this indicates that the interaction between this peptide and the negatively charged membranes is mainly electrostatic and occurs at the membrane surface, with no significant penetration in the lipid's hydrocarbon core.

For these two membrane systems with high PG content, the CG-MD results show that the predominant interaction between all CPs and both membranes is electrostatic, as can be clearly visualized from the number of contacts of the individual residues (Fig. 4, columns 3-4). However, in the case of **CPR**, the system seems to be still evolving towards the typical behavior observed in previous membrane systems, mainly DMPE:DMPG (1:1): a decreasing of Arg-membrane interaction in favor of a correlated increase in the number of contacts through Trp and the adjacent residues in the sequence, Ser and Pg. This indicates that after an initial approach electrostatically driven (with the Arg facing the membrane, interacting with the lipid's headgroups) the peptides rotate turning the Trp towards the lipid chains. As such, based on DSC and MD results we suggest that we possibly have also here a quasi-interdigitated phase for **CPR** and DMPE:DMPG (1:9 and pure DMPG), that can only take place if the apolar part of the peptide's nanotubes face the hydrocarbon chains of the lipid.

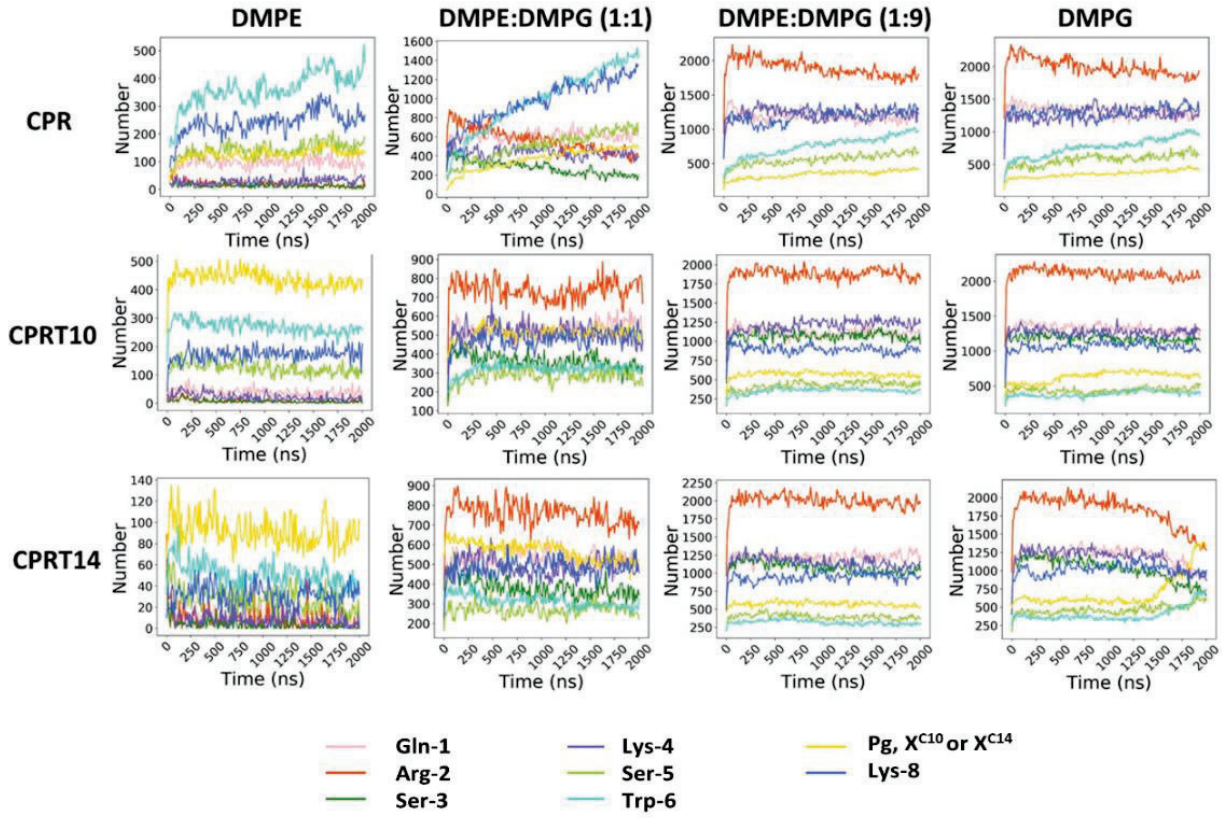

Fig. 4. Number of contacts within 0.6 nm between any pair of atoms of each amino acid of **CPR**, **CPRT10** or **CPRT14** and the corresponding membrane compositions, DMPE, DMPE:DMPG (1:1), DMPE:DMPG (1:9) and DMPG, respectively over 2 microseconds, analyzed from the CG-MD simulations. Note that the scales in all cases are not the same on purpose, to facilitate the visualization of the lines. Matplotlib [52] library was used to produce the figures.

In the case of the other two peptides, **CPRT10** and **CPRT14**, the DSC results for the two PG rich lipid systems must be evaluated separately. Starting for pure DMPG, for **CPRT10** (Fig. 2 B) a small decrease in T_m is observed for the lowest peptide content (27:1). Thereafter, two peaks are superimposed, one centered at T_m of the pure DMPG and another at about 1°C lower (Table S1), showing that the peptide is destabilizing the lipid membrane. As regarding **CPR14** and DMPG (Fig. 2 C), after an initial decrease in T_m of ~1°C for the lowest peptide content, a peak splitting is already present. However, it presents different characteristics – at L:P ratio 22:1 two transitions appear, of just slightly enlarged width as compared to pure lipid, but at the highest peptide content, 12:1, the DSC tracing shows a sharp peak centered around 20 ° that coexists with a broad peak centered about 22°C (see peak deconvolution for these ratios in Fig

S2). These results can be interpreted as showing that at high peptide content part of the membrane most likely forms disk-like peptide aggregates, that undergo a broad transition and coexist with DMPG with small amount of peptide. A similar situation was already described for another antimicrobial peptide, LL-37 by Sevcsik *et al* [33, 51]. The distinctly different behavior of **CPRT10** and **CPRT14** as compared to **CPR** can be ascribed to the presence of the 10 and 14 hydrocarbon tails.

The MD results for DMPG display a strong distortion of the membrane, and also show significant differences between the two peptides with tail. Whereas up to 1 μs the behavior of **CPRT14** is very similar to **CPRT10**, after that the number of contacts between Arg and the membrane significantly decreases, together with an increase in the number of contacts between the T14 tail and the membrane, all this accompanied by a great distortion and final collapse of the membrane system (Fig. 4, column 4 and Fig. 5). These observations match perfectly with the DSC results found for **CPRT14** and DMPG at the highest peptide content, where we concluded that lipid-peptide disks are formed, that lead to membrane disintegration.

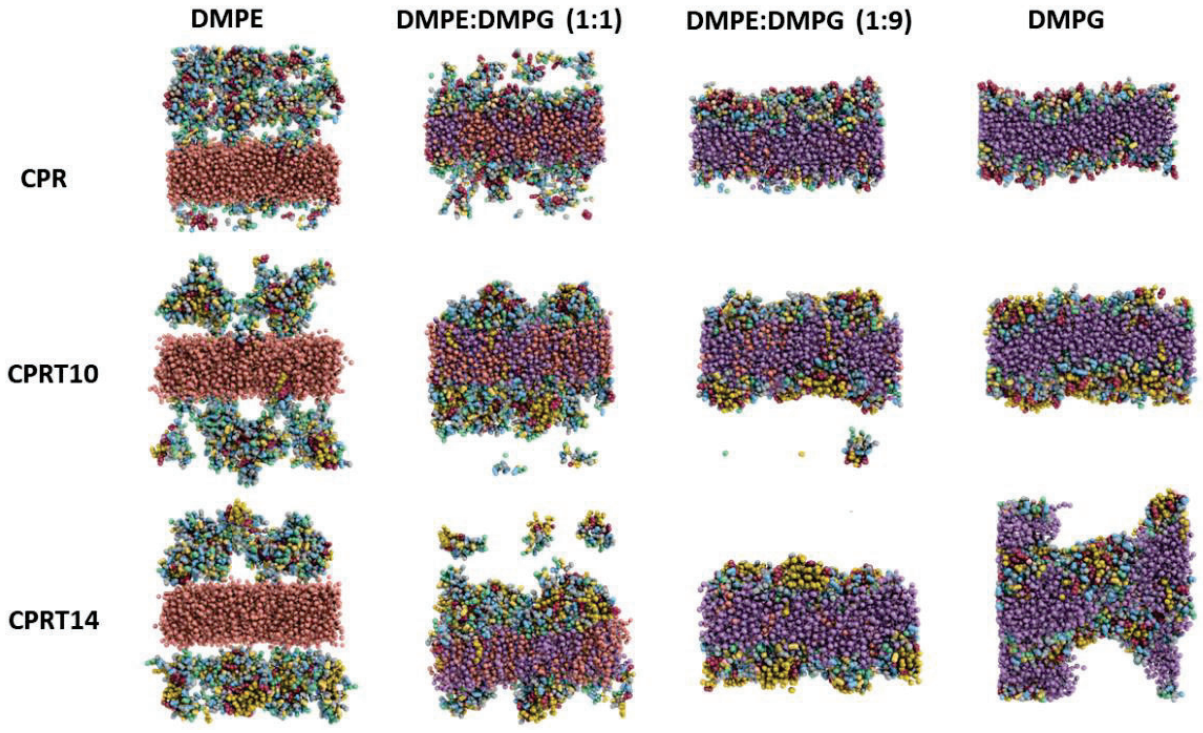

Fig. 5. Lateral view of the last snapshots at t=2 μs from the CG-MD simulation of 160 units of **CPR**, **CPRT10** and **CPRT14**, respectively, in the presence of different membrane compositions: DMPE, DMPE:DMPG (1:1), DMPE:DMPG (1:9) and DMPG. DMPE lipids are represented in orange whereas DMPG lipids are represented in purple. Each residue in the CP is represented in a different color. Water molecules have been removed for clarity. Top view is represented in Fig. S3. The figure was rendered using PyMOL (The PyMOL Molecular Graphics System, Version 2.5 Schrödinger, LLC).

The structural changes in peptide organization and their possible effect on the lipid bilayer's structure were extensively studied by ATR-FTIR by our group for these three peptides, and the initial results obtained for **CPR** and **CPRT10** when mixed with DMPG liposomes were already published [48]. In that study, we reported for both peptides the presence in the amide I band of a peak centered around 1675 cm^{-1} and another at 1625 cm^{-1}, associated with the presence of β-turn [53] and β-sheet [16] structures, respectively. The spectrum also showed a peak for the amide II at 1540 cm^{-1}, representing intermolecularly hydrogen-bonded amide groups together with unbound N-H, providing evidence for nanotube formation in the presence of DMPG membranes [16, 48]. Deconvolution of the peaks revealed in the case of these two peptides the presence of the parallel component of the amide I peak at ~1690 cm^{-1} (weak) together with the perpendicular component (strong) at 1625 cm^{-1}, indicating the possible presence of antiparallel β-sheets. The position of the aggregates as regarding the membrane was derived from the results obtained when using polarized light, where the obtained negative dichroism at 1625 cm^{-1} indicated that the formed structures laid parallel to the membrane plane [48, 54]. Considering the results obtained by MD above, it is possible that the observed dichroism is not too strong as many of the peptides are involved in aggregates, of micellar type, and do not associate into well-formed nanotubes.

When similar measurements were made with **CPRT14** and DMPG, at different L:P ratios, we observe the same type and position of peaks, as reported for **CPR** and **CPRT10** - the amide I band also has two peaks, one around 1675 cm^{-1} and other at 1625 cm^{-1}, associated with the possible presence of β-turn [53] and β-sheet [16] structures, respectively (Fig. 6). Additionally, for higher CP contents, the spectra show a well-defined peak at ~1692 cm^{-1}, indicating the presence of either antiparallel β-sheet structure or aggregated strands [55], and the peak for the amide II at 1540 cm^{-1} is also present. Two interesting observations for this system should be referred: i) the peak at 1625 cm^{-1} has higher intensity for the middle L:P ratio, 23:1 when compared to L:P 10:1 and further ii) the peak at 1625 cm^{-1} is higher than the peak at 1675 cm^{-1} for L:P 23:1 while the opposite is observed for 10:1. These can be associated with the formation of new (possibly aggregated) structures. This is in line with both the DSC results, where we observe a decrease in the T_m and clear domain formation with increase in peptide content, and with the MD results, which suggest the formation of self-assembled/aggregated structures, and that interact with the membrane while partly maintaining the micellar aggregates. In parallel with treatment in our previous publication [48], we did also here a curve fitting to deconvolute the observed peaks in the range 1800–1600 $cm^{-1}$for **CPRT14**. This deconvolution allowed us to estimate the percentage of the various β-structures present, as indicative values, and the values retrieved were 80% β-sheet and 22% of β-turns/aggregated structures for **CPR**, as opposed to 46% of β-sheet and 54% of β-turns/aggregated structures and 40% of β-sheet and 60% of β-turns/aggregated structures for **CPRT10** and **CPRT14**, respectively. These results fit very well with what was found here by MD, where **CPR** formed predominantly nanotubes with β-sheet structure as opposed

to the peptides with tail, that induced domain formation within the lipid membrane, composed of lipid and micellar-like aggregates at high peptide contents. Finally, it is worth mentioning that the self/association of **CPRT10** and **CPRT14** was experimentally verified by González-Freire *et al* [32] by fluorescence measurements with thioflavin T (ThT), obtaining critical aggregation values of ~13 μM and ~4.5 μM for **CPRT10** and **CPRT14,** respectively.

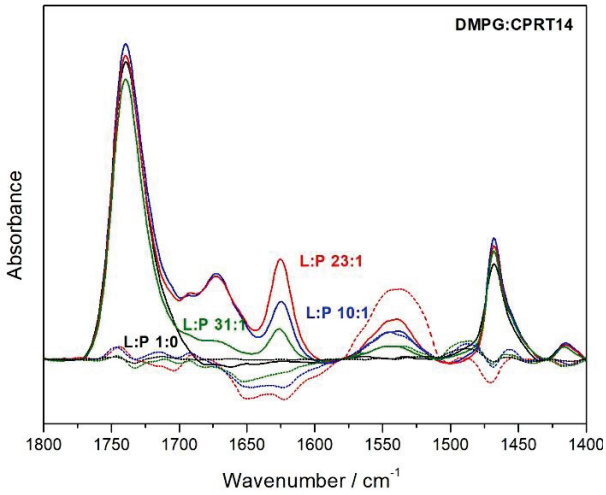

Fig. 6. ATR-FTIR results for DMPG (black line, L:P 1:0) and its mixtures with **CPRT14**. The different molar ratios for the mixtures, L:P, are shown in each curve. The dichroic spectra for the various ratios (dashed lines, same color code) are also shown and calculated as the difference between the parallel and perpendicular spectra, with appropriate scaling. Note that the negative dichroism at 1465 cm^{-1} (ν_{δ} (CH_2) with dipole perpendicular to the chain) also confirms that the membranes are oriented parallel to the support, as stated in the text.

A qualitative analysis of the orientation of the nanotubes or aggregated structures was obtained through the use of ATR-FTIR with polarized light. The orientation as regarding the membrane plane was evaluated by subtracting spectra recorded with the perpendicular incident light from spectra obtained with the parallel incident light (|| - ⊥), multiplied by an appropriate factor [56]. Negative deviations of the difference spectra at 1625 cm^{-1} (dashed lines, Fig. 6), whose intensity increases with increasing peptide content, indicates that the peptide C=O bond arranges perpendicular to the membrane normal axis - the nanotubes are thus oriented parallel to the membrane normal axis. The positive dichroism of the amide II peak (1540 cm^{-1}) (Fig. 6) is also in line that orientation [54, 56].

When DMPE and DMPG are mixed, DSC shows as expected a broader profile in the transition curve, due to structural mismatch between the two lipids. However, at pH 7.45, the formation of ion pairs facilitates PE headgroup's hydration, stabilizing the lipid mixture [49]. For the two peptides with tail, **CPRT10** and **CPRT14,** the effect of decreasing the membrane's negative charge by adding a zwitterionic lipid at DMPE:DMPG (1:9) can be seen in Fig. 2E,F. Both peptides induce a clear segregation in the membrane, with the appearance of peaks at lower temperatures. Again here, some differences exist between **CPRT10** and **CPRT14** – for **CPRT10** the peak around 25ºC is maintained (peptide poor domain), with a small increase in width as the peptide content increases, and a peak at lower temperature appears (peptide-rich), which temperature decreases for the highest peptide content, but its relative importance in terms of enthalpy is maintained; for **CPRT14** the main peak maintained, whereas the peptide-rich part of the membrane appears to be formed by 'patches' of different composition, as more than one peak appears at lower temperatures. These differences reflect both a longer hydrocarbon tail, that drives a larger partition of **CPRT14** to the lipid membranes, and the capacity of this peptide to also interact with DMPE (see below). Overall, the observed peak splitting reflects in the preferential association of the positively charged CPs with DMPG, as the new low temperature peaks move towards temperatures close to the T_m for DMPG (23.2ºC) (they are thus richer in peptide and DMPG), whereas the remaining mixture (richer in PE:PG with some associated CP), has peaks at temperatures similar to the original lipid mixture. The ability of linear and cyclic peptides to induce segregation and domain formation within PE:PG membranes has been reported by our group for different CPs, as well as by other groups using different antimicrobial peptides [13, 44, 57].

The CG-MD results also did not show large differences for the interactions of **CPRT10** and **CPRT14** with DMPE:DMPG (1:9), except for a slightly higher number of Arg-membrane contacts in the case of **CPRT14** (Fig. 4).

The structural effect of the peptides by ATR-FTIR in the presence of DMPE:DMPG (1:9) can be seen in Supplementary material Fig. S9. In Fig. 7 we show the spectra for the three CPs in DMPG and DMPE:DMPG (1:9) at a chosen L:P molar ratio, L:P 10:1, to compare the influence of the membrane charge in the structure and nanotube/aggregates' formation. When we compare the relative intensities, we see that overall, there is a trend in peak intensity depending on peptide, being the peaks for **CPR** the highest, followed by **CPRT10** and then **CPRT14**. Indeed, this reflects the fact found by MD that **CPR** forms mainly nanotubes at the lipid surface, whereas **CPRT10** and **CPRT14** form mainly micellar aggregates, with few nanotubes.

When we add 10% of DMPE to the negatively charged DMPG (Fig. 7 B) we observe the presence of the same peaks in the amide I and amide II band, but two striking differences are apparent - the increase in

intensity of the 1625 cm^{-1} peak for all peptides, this peak becoming more intense than the one at 1675 cm^{-1} in the same amide band, and the decrease in the intensities for the C=O 1740 cm^{-1} for the mixture with **CPRT14**. Indeed, this points to the presence of other aggregated structures, as the peaks at 1675 cm^{-1} and 1692 cm^{-1} (β-turns or antiparallel β-sheet or aggregated strands [55]) are evident, in line with our DSC observation of a peak splitting (see above DSC section) and the MD results above for **CPRT10** and **CPRT14**. The decrease in the intensity of the C=O band (1740 cm^{-1}) and the peak at 1675 cm^{-1} for DMPE:DMPG (1:9):**CPRT14**, may indicate the presence of aggregates/other type of structures, associated with peptide micellar state, as already stated above, as well as the partial destruction of the lipid membrane. Again, these observations are in line with the DSC and MD findings, as we observe some membrane segregation, with parts of the membrane richer in DMPG and peptide, and other parts richer in DMPE.

Overall, as regarding the position of the macromolecular structures relative to the membranes, obtained from the polarized spectra for lipid systems here studied (results not shown), the negative dichroism indicates that the nanotubes structures formed by **CPR** as well as the aggregates formed by **CPRT10** and **CPRT14** lay parallel to the membrane, thus adopting the same orientation already reported in the presence of DMPG membranes in previous studies [48] and here for **CPRT14**.

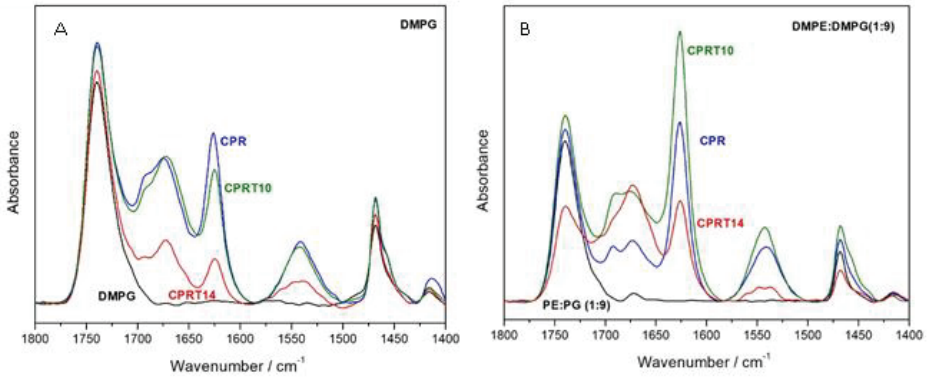

Fig. 7. ATR-FTIR results for **CPR**, **CPRT10** and **CPRT14** mixed with DMPG (A) and DMPE:DMPG(1:9) (B), at L:P 10:1 molar ratio. The color code for the different spectra is: pure lipid (black), and mixtures with **CPR** (blue), with **CPRT10** (green) and **CPRT14** (red).

DMPE:DMPG (1:1) model membrane

When the content in DMPE is further increased (lower negative charge content), a peak with increased T_m can be observed in the DSC tracings of the three CPs. This reflects most likely the depletion of DMPG from part of the membrane, leaving a lipid mixture with composition that approaches DMPE as the CP

content increases (Fig. 2 G-I). In the case of **CPRT10** and **CPRT14** a second, low temperature peak is clearly seen, close to the T_m of pure DMPG (Fig. 2H,I and Table S1), showing that these two peptides induce a clear phase separation in DMPE:DMPG (1:1) mixtures. As a result, we have DMPG-rich regions (low temperature peak) in equilibrium with the remaining membrane mainly composed mainly of DMPE, possibly still with some DMPG and CP associated (higher temperature peak), as its transition temperature is lower than the one we determined to pure DMPE membranes, 50.3 ºC. This behavior has been reported for different antimicrobial peptides [13, 58, 59].

The MD results show that the influence of DMPE is still significant for the membrane system DMPE:DMPG (1:1) (Fig. 5, Fig. S4-S6). The number of contacts between all CPs and DMPE:DMPG (1:1) substantially increases when compared to the pure DMPE membrane (see above, Fig. 4, second column), showing the importance of DMPG on the interaction.

A clear difference is again found in the behavior of **CPR** when compared to the peptides bearing the hydrocarbon tails, **CPRT10** and **CPRT14**: in the case of **CPR** the interaction with the membrane is dominated by the Trp and the Lys adjacent to the Pg residue, whereas the highest number of contacts between **CPRT10** and **CPRT14** and the DMPE:DMPG (1:1) corresponds to the Arg residue (Fig. 4, second column). Interestingly, as can be observed from the graphics, the interaction with Arg was also prevalent for **CPR** at this membrane composition at the beginning of the CG-MD simulation, but as the simulation progresses, these Arg-membrane contacts are replaced by the interaction with Trp and Lys mentioned previously. Overall, the common aspects for the peptide/membrane interaction, namely electrostatic interactions and the role of Trp in the membrane anchoring, are in line with the expected behavior for AMPS [34], and were also observed with other CPs in previous works [13]. The electrostatic interaction between the charged residues of the CP and the charged heads of the lipids are the driving force attracting the peptides towards the membrane, where thereafter the peptides turn around, inserting their hydrophobic residues into the membrane. What is remarkable is how clear this shows up in the **CPR** simulation results (Fig. 4). It is also noteworthy that once this happens, the number of contacts between Trp and Lys and the membrane significantly increase (up to 1200-1400, and they seem to be still evolving) with respect to the initial electrostatic contacts between Arg and the membrane, suggesting that this interaction is much more favorable, *i.e.*, energetically more stable. In the case of **CPRT10** and **CPRT14** the electrostatic interaction with the membrane takes place mainly through the Arg charged residues in the first steps of the simulation. However, it should be noted that within the simulated time (2 μs), most of **CPRT10** and **CPRT14** units are not able to turn around and introduce their hydrophobic tails inside the membrane, at odds with **CPR**, as clearly seen in Fig. 4. In fact, as it can be appreciated in Fig. 4, although the main membrane interaction between **CPRT10** and **CPRT14** takes place through the Arg

residue, there are some contacts with the DMPE:DMPG (1:1) membrane through the T10 and T14 tails already at this simulation time. The insertion of the hydrophobic tails in the membrane involves breaking the micellar aggregates and this behavior could not be observed within the simulation times studied here. However, the extension of some of the CG-MD simulations for longer periods (20 μs), led indeed, to much more tails inserted in the membrane (see an example for **CPRT10** and **CPRT14** in Fig. S7-S8). These finding are in agreement with the DSC results, as the strong interaction of **CPRT10** and **CPRT14** with DMPG leads to segregation and to the appearance of DMPE-rich and DMPE-poor domains within the membrane.

The ATR-FTIR results for this system (Fig. 8) show the same peaks and similar decrease in the intensity of C=O band (1740 cm^{-1}) for all CPs, as described above for the system DMPE:DMPG (1:9). In the case of **CPR**, the spectra suggest that most self-assembled structures are *β*-sheet type, as we have a low intensity peak at 1625 cm^{-1}, in agreement with the MD results. Again, for this model membrane system, the spectra for **CPRT14** suggest the presence of aggregates/other type of structures, in agreement with the DSC and MD results. Further, these findings also in line with the observation for **CPRT14** of an arrangement of self-assembled peptides with a filamentous structure, in the studies of González-Freire *et al*, when the peptides were studied in a solution (without membranes) by STEM microscopy [32].

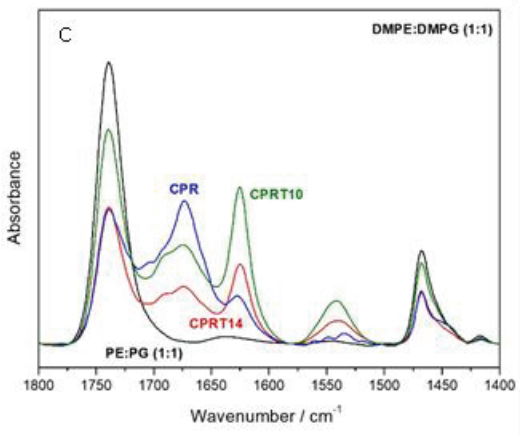

Fig. 8. ATR-FTIR results for **CPR**, **CPRT10** and **CPRT14** mixed with DMPE:DMPG(1:1) at L:P 10:1 molar ratio. The color code for the different spectra is: pure lipid (black), and mixtures with **CPR** (blue), with **CPRT10** (green) and **CPRT14** (red).

DMPE model membrane

The DSC results show that **CPR** hardly interacts with DMPE (Fig. 2J), whereas **CPRT10** shows a clear but small change in the thermal profile, that is not strong enough to be reflected in a significant change in

thermodynamic parameters (see Table S1). In the case of **CPRT14** the $\Delta_{trans}H$ decreases significantly with L:P decrease, indicating that this peptide interacts with this zwitterionic lipid. Nevertheless, it is difficult to interpret the observed effect on the DSC profile, mostly a decrease in Δ_{trans}H, and no change in T_m, as one would expect if the tails or hydrophobic moieties of the peptide would penetrate the hydrophobic core the DMPE.

A feature common to all simulations carried out in presence of DMPE is that there is very little (**CPRT10** and **CPRT14**) on no (**CPR**) insertion of the peptides into the membrane (Fig. 5 and Fig. S3-S6). These computational findings support the conclusions above from the DSC results. The MD results can provide us further detail on these weak interactions. Regarding the differences between the three peptides in the presence of this membrane model, the peptides with the tail continue to associate mostly into micellar aggregates (**CPRT14** and **CPRT10**) as in solution, whereas **CPR** forms short nanotubes. Some (few) peptides **CPRT10** and **CPRT14** bury the aliphatic tail and the adjacent Trp in the membrane, either through isolated CP units or through small nanotubes over the surface (Fig. 5 and Fig. S4-S6). The interaction of **CPR** with the DMPE membrane takes place mostly through the residues Trp and Lys adjacent to Pg (bearing the alkyne moiety) (Fig. 4). The presence of T10 tail significantly increases the number of contacts between **CPRT10** and DMPE membrane, through this hydrocarbon moiety, together with the neighboring Trp, as well as through the adjacent Lys to a minor extent (Fig. 4 and Fig. S5). The longest tail, however, drastically reduces the number of contacts between **CPRT14** and the DMPE membrane (Fig. 4 and Fig. S6). Although the residues interacting mostly with the membrane are the same as for **CPRT10** (the hydrocarbon tail, Trp and the adjacent Lys), the number of interactions shows a significant decrease (about 4 times less than the previous peptide).

DMPC model membrane

Finally, the interaction of the three peptides with DMPC was also tested by DSC, as this membrane system is often used as a simplified model membrane for eukaryotic cells, as a remarkable parallelism between toxicity and interaction with DMPC membranes has been shown [26, 34, 37, 39, 60]. The results show that **CPR** does not interact at all with this membrane system, whereas **CPRT10** and **CPRT14** show a mild interaction (Fig. S1 and Table S2).

CONCLUSIONS

This work presents an orthogonal study using biophysical experiments (DSC and ATR-FTIR) and CG-MD simulations of peptide/lipid model membranes mimicking bacteria membranes, aiming at

understanding the mechanism of action of second generation D,L-α-cyclic peptides, with proven antimicrobial activity. The CPs here studied share the same sequence but differ in the presence of a hydrophobic tail of ten (**CPRT10**) or fourteen (**CPRT14**) carbons that replaces a Pg in the original sequence (**CPR**).

DSC results showed that the presence of negative charge in the membrane is a requirement for a strong interaction of the three peptides, as **CPR** and C**PRT10** do not interact and **CPRT14** just weakly with the zwitterionic DMPE. Further, it is shown that the interaction depends on charge content and on peptide, being stronger for the cyclic peptides with a tail and for the more negatively charged membranes. Importantly, the CG-MD results show that the macromolecular structures adopted by the three peptides are different – mostly short nanotubes in the case of **CPR**, and mainly micellar-type aggregates in the case of **CPRT10** and **CPRT14**, in line with results presented by González-Freire et al [32]. These finding corroborate the interpretations we suggest for the observed DSC profiles, showing a distinct behavior of **CPR** as compared to the other two peptides with tail. This is also supported by our FTIR-ATR results, where the amide I band peaks and the peak for the amide II, associated with the presence of β-sheet/aggregated structures and intermolecularly interactions respectively, are present for all three CPs. Further, they show that there is a trend in peak intensity depending on peptide, being the peaks for **CPR** the highest, followed by **CPRT10** and then **CPRT14**, related to the formation of a lower number of nanotubes in the case of **CPRT10** and **CPRT14** when compared to **CPR**. Finally, these results can help the understanding of the antimicrobial activity found for these peptides - very weak for **CPR**, very active and fast for **CPRT10**, and very active but somewhat slower for **CPRT14**. Although **CPR** is also interacting strongly to the negatively charged membranes, it is not destructive, as it shows a mild degree of membrane penetration and no significant segregation in mixed membranes. On the contrary, the two peptides with tail have a strong electrostatic interaction with negatively charged membranes, leading to membrane disintegration at high peptide contents in the case of **CPRT14** (with peptide lipid discs formation, detergent like behavior), and to extensive domain formation in the case of **CPRT10.** For less negatively charged mixed membranes, both peptides induce membrane segregation, that must impair cell function in real pathogen systems. The observed faster effect of **CPRT10** as compared to **CPRT14** may be due to the weaker tendency of this peptide to form micellar aggregates, making its partition to the membrane more favorable and faster.

ACKNOWLEDGMENTS

M.B., B.C., A. P. and R. G. F. acknowledge the financial support from Fundação para a Ciência e Tecnologia (FCT), Portugal, for a PhD grant PD/BD/135095/2017 (to B.C.), and FCT national funds and

FEDER European funds, through COMPETE2020 program, project PTDC/BIA-BFS/30579/2017 (POCI-01-0145-30579) and UIDB/00081/2020. R.G.F. acknowledges to the Spanish Agencia Estatal de Investigación (AEI) and the ERDF (RTI2018-098795-A-I00), and to the Xunta de Galicia and the ERDF (ED431F 2020/05, ED431C 2017/25 and Centro singular de investigación de Galicia accreditation 2016-2019, ED431G/09). R.G.-F. thanks to Ministerio de Ciencia, Innovación y Universidades for a "Ramón y Cajal" contract (RYC-2016-20335). B.C. acknowledges a STSM grant from COST Action CA15126 "Between Atom and Cell: Integrating Molecular Biophysics Approaches and Health Care (MOBIEU), for a research stay in Brussels, Belgium, at E. G.'s Lab. M.B. and B.C. thank Profs. Paula Gameiro and Eulália Pereira for the access to the DLS instrument. E.G. is Research Director with the National Fund for Scientific Research (Belgium). All the calculations were done at CESGA.

ABBREVIATIONS

CPs, cyclic peptides; SCPNs, cyclic peptide nanotubes; AMPs, antimicrobial peptides; MD, molecular dynamics; CG, coarse-grained resolution; DSC, differential scanning calorimetry; ATR-FTIR, attenuated total reflection Fourier – infrared spectroscopy; Pg, propargylglycine group; DMPE, 1,2-dimyristoyl-sn-glycero-3-phosphoethanolamine; DMPG, 1,2-dimyristoyl-sn-glycero-3-phospho-(1'-rac-glycerol); DMPC, 1,2-dimyristoyl-sn-glycero-3-phosphocholine; PE, phosphoethanolamine; PG, phospho-(1'-rac-glycerol); T_m, transition temperature; *Cp*, heat capacity; Gln, Glutamine; Arg, Arginine ; Ser, Serine; Lys, Lysine; Trp, Tryprophan; DCM, dichloromethane; HPLC, High-Performance Liquid Chromatography; HEPES, 4-(2-hydroxyethyl)-1- piperazineethanesulfonic acid; EDTA, Ethylenediamine tetra-acetic acid; FMOC, fluorenylmethoxycarbonyl protecting group; LUVs, Large unilamellar vesicles;

REFERENCES

[1] I. A. Banerjee, L. Yu, H. Matsui, Location-Specific Biological Functionalization on Nanotubes: Attachment of Proteins at the Ends of Nanotubes Using Au Nanocrystal Masks, Nano Lett. 3 (2003) 283-287.

[2] C. Cheng, C. Zhang, X. Gao, Z. Zhuang, C. Du, W. Chen, 3D Network and 2D Paper of Reduced Graphene Oxide/Cu2O Composite for Electrochemical Sensing of Hydrogen Peroxide, Anal. Chem. 90 (2018) 1983-1991.

[3] M.R. Ghadiri, J.R. Granja, R.A. Milligan, D.E. McRee, N. Khazanovich, Self-assembling organic nanotubes based on a cyclic peptide architecture, Nature 366 (1993) 324-327.

[4] Q. Hu, H. Li, L. Wang, H. Gu, C. Fan, DNA Nanotechnology-Enabled Drug Delivery Systems, Chem. Rev. 119(10) (2019) 6459-6506.

[5] A.O. Oluwole, B. Danielczak, A. Meister, J.O. Babalola, C. Vargas, S. Keller, Solubilization of Membrane Proteins into Functional Lipid-Bilayer Nanodiscs Using a Diisobutylene/Maleic Acid Copolymer, Angew. Chem. Int. Ed. 56 (2017) 1919-1924.
[6] M.C. Roco, Nanotechnology: convergence with modern biology and medicine, Curr. Opin. Biotechnol. 14 (2003) 337-346.
[7] A. Ivankin, L. Livne, A. Mor, G.A. Caputo, W.F. DeGrado, M. Meron, B. Lin, D. Gidalevitz, Role of the Conformational Rigidity in the Design of Biomimetic Antimicrobial Compounds, Angew. Chem. Int. Ed. 49 (2010) 8462-8465.
[8] S. Keller, I. Sauer, H. Strauss, K. Gast, M. Dathe, M. Bienert, Membrane-Mimetic Nanocarriers Formed by a Dipalmitoylated Cell-Penetrating Peptide, Angew. Chem. Int. Ed. 44 (2005) 5252-5255.
[9] M. Xiong, Z. Han, Z. Song, J. Yu, H. Ying, L. Yin, J. Cheng, Bacteria-Assisted Activation of Antimicrobial Polypeptides by a Random-Coil to Helix Transition, Angew. Chem. Int. Ed. 56 (2017) 10826-10829.
[10] V.S. Bystrov, I.K. Bdikin, A. Heredia, R.C. Pullar, E.D. Mishina, A.S. Sigov, A.L. Kholkin, Piezoelectricity and ferroelectricity in biomaterials: from proteins to self-assembled peptide nanotubes, Piezoelectric nanomaterials for biomedical applications, Springer, 2012.
[11] I.W. Hamley, Soft Matter Nanotechnology. From Structure to Function Edited by Xiadong Chen and Harald Fuchs, . Angew. Chem. Int. Ed. 55 (2016) 3262-3262.
[12] R.V. Ulijn, A.M. Smith, Designing peptide based nanomaterials, Chem. Soc. Rev. 37 (2008) 664-675.
[13] B. Claro, E. González-Freire, M. Calvelo, L.J. Bessa, E. Goormaghtigh, M. Amorín, J.R. Granja, R. Garcia-Fandiño, M. Bastos, Membrane targeting antimicrobial cyclic peptide nanotubes – an experimental and computational study, Colloids Surf. B - Biointerfaces (2020) 111349.
[14] S. Fernandez-Lopez, H.-S. Kim, E.C. Choi, M. Delgado, J.R. Granja, A. Khasanov, K. Kraehenbuehl, G. Long, D.A. Weinberger, K.M. Wilcoxen, M.R. Ghadiri, Antibacterial agents based on the cyclic d,l-[alpha]-peptide architecture, Nature 412 (2001) 452-455.
[15] J.D. Hartgerink, J.R. Granja, R.A. Milligan, M.R. Ghadiri, Self-Assembling Peptide Nanotubes, J. Am. Chem. Soc. 118 (1996) 43-50.
[16] H.S. Kim, J.D. Hartgerink, M.R. Ghadiri, Oriented Self-Assembly of Cyclic Peptide Nanotubes in Lipid Membranes, J. Am. Chem. Soc. 120 (1998) 4417-4424.
[17] S. Hernando-Amado, T.M. Coque, F. Baquero, J.L. Martínez, Defining and combating antibiotic resistance from One Health and Global Health perspectives, Nature Microbiol.4 (2019) 1432-1442.
[18] P. Kumar, J.N. Kizhakkedathu, S.K. Straus, Antimicrobial Peptides: Diversity, Mechanism of Action and Strategies to Improve the Activity and Biocompatibility In Vivo, Biomolecules 8 (2018) 24.

[19] O. Fleitas, O.L. Franco, Induced Bacterial Cross-Resistance toward Host Antimicrobial Peptides: A Worrying Phenomenon, Front. Microbiol. 7 (2016) 381-381.
[20] R.I. Lehrer, T. Ganz, Antimicrobial peptides in mammalian and insect host defence, Curr. Opin. Immunol. 11 (1999) 23-27.
[21] J.T. Mika, G. Moiset, A.D. Cirac, L. Feliu, E. Bardaji, M. Planas, D. Sengupta, S.J. Marrink, B. Poolman, Structural basis for the enhanced activity of cyclic antimicrobial peptides: the case of BPC194, Biochim. Biophys. Acta 1808(9) (2011) 2197-205.
[22] L.A. Calderon, A.M. Soares, R.G. Stábeli, Anuran Antimicrobial Peptides: an alternative for the development of nanotechnological based therapies for multi-drug-resistant infections, Signpost. Open J. Biochem. Biotech. 1 (2012) 1-11.
[23] C.D. Fjell, J.A. Hiss, R.E. Hancock, G. Schneider, Designing antimicrobial peptides: form follows function, Nat. Rev. Drug Discovery 11 (2011) 37-51.
[24] W.C. Wimley, K. Hristova, Antimicrobial peptides: successes, challenges and unanswered questions, J. Membr. Biol. 239 (2011) 27-34.
[25] Brogden, K. A. Antimicrobial peptides: pore formers or metabolic inhibitors in bacteria? Nature rev. microbiol. 3 (2005), 238.
[26] T. Silva, R. Adão, K. Nazmi, J.G.M. Bolscher, S.S. Funari, D. Uhríková, M. Bastos, Structural diversity and mode of action on lipid membranes of three lactoferrin candidacidal peptides, Biochim. Biophys. Acta, Biomembr. 1828 (2013) 1329-1339.
[27] V. Teixeira, M.J. Feio, M. Bastos, Role of lipids in the interaction of antimicrobial peptides with membranes, Prog. Lipid Res. 51 (2012) 149-177.
[28] R.J. Brea, C. Reiriz, J.R. Granja, Towards functional bionanomaterials based on self-assembling cyclic peptide nanotubes, Chem. Soc. Rev. 39 (2010) 1448-1456.
[29] R. García-Fandiño, M. Amorín, L. Castedo, J.R. Granja, Transmembrane ion transport by self-assembling α,γ-peptide nanotubes, Chem. Sci. 3 (2012) 3280-3285.
[30] W.S. Horne, C.M. Wiethoff, C. Cui, K.M. Wilcoxen, M. Amorin, M.R. Ghadiri, G.R. Nemerow, Antiviral cyclic d,l-α-peptides: Targeting a general biochemical pathway in virus infections, Bioorg. Med. Chem. 13 (2005) 5145-5153.
[31] R.-V. Nuria, H.L. Ozores, G. Arcadio, G.-F. Eva, F. Alberto, P. Michele, M.P. Juan, O. Juan, M. Javier, G.-F. Rebeca, A. Manuel, R.G. Juan, Membrane-Targeted Self-Assembling Cyclic Peptide Nanotubes, Curr. Trends Med. Chem. 14 (2014) 2647-2661.
[32] E. González-Freire, F. Novelli, A. Pérez-Estévez, R. Seoane, M. Amorín, J.R. Granja, Double orthogonal click reactions for the development of antimicrobial peptide nanotubes, Chem. Eur. J. 27 (2020) 3029 – 3038.

[33] K. Lohner, DSC studies on the modulation of membrane lipid polymorphism and domain organization by antimicrobial peptides, in: M. Bastos (Ed.) Biocalorimetry: foundations and contemporary approaches. CRC Press, Boca Raton 2016, chapter 9.
[34] F. Abrunhosa, S. Faria, P. Gomes, I. Tomaz, J.C. Pessoa, D. Andreu, M. Bastos, Interaction and Lipid-Induced Conformation of Two Cecropin−Melittin Hybrid Peptides Depend on Peptide and Membrane Composition, J. Phys. Chem., B 109(36) (2005) 17311-17319.
[35] R. Adão, K. Nazmi, J.G.M. Bolscher, M. Bastos, C- and N-truncated antimicrobial peptides from LFampin 265 – 284: Biophysical versus microbiology results, J. Pharm. BioAllied Sci.3(1) (2011) 60-69.
[36] M. Bastos, G. Bai, P. Gomes, D. Andreu, E. Goormaghtigh, M. Prieto, Energetics and Partition of Two Cecropin-Melittin Hybrid Peptides to Model Membranes of Different Composition, Biophys. J. 94 (2008) 2128-2141.
[37] J.G. Bolscher, R. Adão, K. Nazmi, P.A. van den Keybus, W. van 't Hof, A.V. Nieuw Amerongen, M. Bastos, E.C. Veerman, Bactericidal activity of LFchimera is stronger and less sensitive to ionic strength than its constituent lactoferricin and lactoferrampin peptides, Biochimie 91 (2009) 123-32.
[38] T. Silva, B. Claro, B.F.B. Silva, N. Vale, P. Gomes, M.S. Gomes, S.S. Funari, J. Teixeira, D. Uhríková, M. Bastos, Unravelling a Mechanism of Action for a Cecropin A-Melittin Hybrid Antimicrobial Peptide: The Induced Formation of Multilamellar Lipid Stacks, Langmuir 34 (2018) 2158-2170.
[39] V. Teixeira, M.J. Feio, L. Rivas, B.G. De la Torre, D. Andreu, A. Coutinho, M. Bastos, Influence of Lysine Nε-Trimethylation and Lipid Composition on the Membrane Activity of the Cecropin A-Melittin Hybrid Peptide CA(1−7)M(2−9), J. Phys. Chem., B 114 (2010) 16198-16208.
[40] L.Carpino, A.; G. Y. Han, 9-Fluorenylmethoxycarbonyl function, a new base-sensitive amino-protecting group. J. Am. Chem. Soc. 92 (1970) 5748-5749.
[41] V. Dartois.; J. Sanchez-Quesada; E.Cabezas; Chi, E.; C. Dubbelde; C. Dunn; J. Granja; C. Gritzen; D. Weinberger; M. R. Ghadiri; Jr T. R. Parr, Systemic antibacterial activity of novel synthetic cyclic peptides. Antimicrob. Agents Chemother 49 (2005) 3302-10.
[42] J. M. Palomo, Solid-phase peptide synthesis: an overview focused on the preparation of biologically relevant peptides. RSC Advances 4 (2014) 32658-32672.
[43] P. Rovero, L. Quartara, G. Fabbri, Synthesis of cyclic peptides on solid support, Tetrahedron Letters, 32 (1991) 2639-2642.
[44] S. Finger, A. Kerth, M. Dathe, A. Blume, The efficacy of trivalent cyclic hexapeptides to induce lipid clustering in PG/PE membranes correlates with their antimicrobial activity, Biochim. Biophys. Acta, Biomembr., 1848 (2015) 2998-3006.

[45] S.J. Marrink, H.J. Risselada, S. Yefimov, D.P. Tieleman, A.H. de Vries, The MARTINI Force Field: Coarse Grained Model for Biomolecular Simulations, J. Phys. Chem. B 111 (2007) 7812-7824.
[46] L. Monticelli, S.K. Kandasamy, X. Periole, R.G. Larson, D.P. Tieleman, S.-J. Marrink, The MARTINI Coarse-Grained Force Field: Extension to Proteins, J. Chem. Theory Comput. 4 (2008) 819-834.
[47] D.H. de Jong, G. Singh, W.F.D. Bennett, C. Arnarez, T.A. Wassenaar, L.V. Schäfer, X. Periole, D.P. Tieleman, S.J. Marrink, Improved Parameters for the Martini Coarse-Grained Protein Force Field, J. Chem. Theory Comput. 9 (2013) 687-697.
[48] B. Claro, E. Goormaghtigh, M. Bastos, Attenuated total reflection Fourier transform infrared spectroscopy: a tool to characterize antimicrobial cyclic peptide/membrane interactions, Eur. Biophys. J., S. Ed. dedicated to COST Action CA15126, MOBIEU: Between atom and cell, 2020.
[49] P. Garidel, A. Blume, Miscibility of phosphatidylethanolamine-phosphatidylglycerol mixtures as a function of pH and acyl chain length, Eur.Biophys. J., 28 (2000) 629-638.
[50] G. Pabst, S.L. Grage, S. Danner-Pongratz, W. Jing, A.S. Ulrich, A. Watts, K. Lohner, A. Hickel, Membrane thickening by the antimicrobial peptide PGLa, Biophys J, 95 (2008) 5779-5788.
[51] E. Sevcsik, G. Pabst, A. Jilek, K. Lohner, How lipids influence the mode of action of membrane-active peptides, Biochim. Biophys. Acta, Biomembr., 1768 (2007) 2586-2595.
[52] J.D. Hunter, Matplotlib: A 2D Graphics Environment, Comput. Sci. Eng., 9 (2007) 90-95.
[53] S.A. Tatulian, Structural Characterization of Membrane Proteins and Peptides by FTIR and ATR-FTIR Spectroscopy, in: J.H. Kleinschmidt (Ed.) Lipid-Protein Interactions: Methods and Protocols, Humana Press, Totowa, NJ, 2013.
[54] E. Goormaghtigh, V. Raussens, J.-M. Ruysschaert, Attenuated total reflection infrared spectroscopy of proteins and lipids in biological membranes, Biochim. Biophys. Acta, Rev. Biomembr, 1422 (1999) 105-185.
[55] L.K. Tamm, S.A. Tatulian, Infrared spectroscopy of proteins and peptides in lipid bilayers, Q. Rev. Biophys., 30 (1997) 365-429.
[56] B. Bechinger, J.-M. Ruysschaert, E. Goormaghtigh, Membrane helix orientation from linear dichroism of infrared attenuated total reflection spectra, Biophys. J., 76 (1999) 552-563.
[57] A. Arouri, M. Dathe, A. Blume, Peptide induced demixing in PG/PE lipid mixtures: A mechanism for the specificity of antimicrobial peptides towards bacterial membranes?, Biochim. Biophys. Acta, Biomembr., 1788 (2009) 650-659.
[58] R. Adão, P.F. Cruz, D.C. Vaz, F. Fonseca, J.N. Pedersen, F. Ferreira-da-Silva, R.M.M. Brito, C.H.I. Ramos, D. Otzen, S. Keller, M. Bastos, DIBMA nanodiscs keep α-synuclein folded, Biochim. Biophys. Acta, Biomembr., 1862 (2020) 183314.

[59] A. Blume, Temperature induced and isothermal phase transitions of pure and mixed lipid bilayer membranes studied by DSC and ITC, in: M. Bastos (Ed.) Biocalorimetry: foundations and contemporary approaches. CRC Press, Boca Raton 2016, chapter 6
[60] R. Adão, R. Seixas, P. Gomes, J.C. Pessoa, M. Bastos, Membrane structure and interactions of a short Lycotoxin I analogue, J. Pept. Sci., 14 (2008) 528-534.